Preliminary assessment of the NOAA-21 VIIRS on-orbit Reflective Solar Band calibration and performance

Taeyoung Choi[a,b*], Slawomir Blonski[a,b], Xi Shao[c,b], Wenhui Wang[c,b]

[a] Global Science & Technology (GST), Inc., 7855 Walker Dr., Suite 200, Greenbelt, MD 20770, U.S.A.
[b] NOAA Center for Satellite Applications and Research (STAR), 5830 University Research Ct., College Park, MD 20740-3818, U.S.A.
[c]CISESS/ESSIC, University of Maryland, College Park, MD 20740, USA

ABSTRACT

On November 10, 2022, the NOAA-21 (also known as Joint Polar Satellite System (JPSS)-2) Visible Infrared Imaging Radiometer Suite (VIIRS) was successfully launched and operated on-orbit. The NOAA-21 VIIRS is the third VIIRS instrument in the series, following S-NPP and NOAA-20, providing 22 spectral bands that cover a spectral range from 0. 402 μm to 12.5 μm. From the intensive Post Launch Tests (PLTs), the NOAA-21 VIIRS Sensor Data Record (SDR) achieved beta maturity status on Feb. 23, 2023 and is expected to achieve provisional and validated maturity in the next few months, ensuring the performance requirements are met and data are of high quality with on-orbit calibration.

The accuracy of the current NOAA-21 VIIRS Reflective Solar Band (RSB) calibration was limited by in the Solar Diffuser (SD) degradation estimates, which proportionally affect the accuracy of the on-orbit RSB calibration. To achieve the beta maturity status, the SD degradation was omitted from the initial radiometric response analyses, and calculated solar calibration scaling coefficients (F-factors) were extrapolated to the start of the on-orbit operations that marked the onset of the SD degradation.

To mitigate the unexpected SD reflectance variability, a series of yaw maneuvers will be performed as a part of the PLTs during the Intensive Calibration and Validation (ICV) phase. In addition to the yaw points, on-orbit Solar Diffuser Stability Monitor data sets will fill the intermediate angles between the yaw angles. The updated estimates of the SD degradation (H-factors) will be applied in the SD F-factor calculations. Finally, the improved SD F-factors will be compared and validated with vicarious calibration results, such as lunar F-factors. This paper will evaluate the impacts of SD-based calibration updates for NOAA-21 RSBs through assessing the radiometric biases of NOAA-21 VIIRS RSBs relative to NOAA-20 ensuring the radiometric accuracy of the NOAA-21 SDR products.

Keywords: NOAA-21, VIIRS, Post Launch Test, Reflective Solar Band,

1. INTRODUCTION

The Visible Infrared Imaging Radiometer Suite (VIIRS) was designed and developed based on the lessons learned from previous Earth observing sensors, such as the Advanced Very-high Resolution Radiometer (AVHRR) on NOAA's Polar-orbiting Environmental Satellites (POES), the Moderate-resolution Imaging Spectroradiometer (MODIS) on NASA's Earth Observing System (EOS) Terra and Aqua satellites, and the Sea-viewing Wide Field-of-view Sensor (SeaWiFS) onboard SeaStar [1]. The second VIIRS was launched on November 18, 2017, onboard the National Oceanic and Atmospheric Administration-20 (NOAA-20) satellite, following the predecessor that was on-orbit on October 2011 on the Suomi National Polar-orbiting Partnership (S-NPP) satellite [2]. The third version of the VIIRS instrument was successfully launched on November 10, 2023, at 9:49 Universal Time Coordinated (UTC) from the Vandenberg Space Force Base in Lompoc, CA (https://www.nesdis.noaa.gov/next-generation/jpss-2-launch).

Similar to the predecessors, NOAA-21 VIIRS has 14 reflective solar bands, 7 thermal emissive bands, and a day-night band. The reflective solar bands cover a spectral range from 402 nanometers to 2284 nanometers, while the thermal

Earth Observing Systems XXVIII, edited by Xiaoxiong (Jack) Xiong, Xingfa Gu, Jeffrey S. Czapla-Myers, Proc. of SPIE Vol. 12685, 126850Z
 · 0277-786X · doi: 10.1117/12.2677921

emissive bands cover a range from 3,553 nanometers to 12,345 nanometers. The day-night band is a broad panchromatic band that covers a range from 499 nanometers to 890 nanometers. All the VIIRS (SNPP, NOAA-20 and NOAA-21) spectral response characteristics are listed at the National Calibration Center (NCC) website at (https://ncc.nesdis.noaa.gov).

For the reflective solar bands (RSB), VIIRS provides dual gain operation in six bands (M1~M5, and M6). This means that it can operate at two different radiometric levels, which allows for higher sensitivity to low radiance ocean color applications while avoiding saturation at highly reflective targets from land targets and deep convective clouds. Table 1 shows the spatial and spectral characteristics of NOAA-21 VIIRS.

Table 1. NOAA-21 VIIRS radiometric, spectral and spatial parameters (https://ncc.nesdis.noaa.gov/NOAA-21/StandardizedCalibrationParameters.php).

Band	Center Wavelength [nm]	Min. at half maximum [nm]	Max. at half maximum [nm]	Full Width at Half Maximum [nm]	Thuillier [3] based Esun W/[m^2 µm sr]	Spatial Resolution at nadir [m]	Gain State
I1	641.1	601.4	680.7	79.3	1592.5	375	Single
I2	868.0	848.7	887.3	38.6	950.2	375	Single
I3	1612.9	1581.4	1644.5	63.1	245.6	375	Single
M1	411.0	401.3	420.8	19.5	1733.5	750	High/Low
M2	444.9	436.4	453.4	17.0	1940.1	750	High/Low
M3	488.3	478.3	498.4	20.1	1983.9	750	High/Low
M4	555.3	544.7	566.0	21.3	1833.9	750	High/Low
M5	671.4	660.8	681.9	21.1	1502.5	750	High/Low
M6	747.3	739.9	754.7	14.8	1273.4	750	Single
M7	868.3	849.0	887.6	38.6	949.9	750	High/Low
M8	1241.3	1231.1	1251.6	20.6	454.7	750	Single
M9	1382.0	1374.4	1389.7	15.3	362.8	750	Single
M10	1613.1	1581.5	1644.6	63.1	245.6	750	Single
M11	2251.7	2227.7	2275.8	48.0	78.1	750	Single

The primary source of on-orbit radiometric calibration for the VIIRS reflective solar bands (RSB) is the solar diffuser (SD). The SD's bidirectional reflectance distribution function (BRDF) was carefully measured before launch using a National Institute of Standards and Technology (NIST) traceable radiometric source[4]. The on-orbit radiometric calibration coefficients are calculated using the SD measurements, which track changes in the detector response, optical throughput, half-angle mirror (HAM) sides, and scans for all the RSB bands.

Even though the prelaunch SD BRDF was accurately measured, its reflectance has gradually degraded due to exposure to strong ultraviolet (UV) radiation from the sun[5, 6]. The time-dependent reflectance degradation is measured by the periodic operation of the solar diffuser stability monitor (SDSM). As shown in Figures 1 and 2, the SDSM has two viewing ports: the SD port, which views the surface of the SD and tracks degradation of the SD reflectance at a given solar angle; and the sun view port, which measures the incoming solar radiance through the SDSM sun screen, which is a thin steel plate with tiny holes to reduce the strong incoming solar illumination.

Previously, the prelaunch SDSM Sun view screen transmittance Look Up Table (LUT), the τ_{SDSM} in Figure 2, was incorrectly measured. It caused large oscillations up to 1.5 percent when measuring the on-orbit SD degradation especially with the SDSM detector 7. Alternately, a new version of the τ_{SDSM} LUT was derived using yaw maneuver data sets and on-orbit SDSM data. The long-term SD degradations (or called H-factors) were significantly improved by reducing Sun screen oscillations especially in the solar azimuth angles [7, 8]. Similar oscillation patterns were also observed after performing the 15 orbit yaw maneuvers from March 6-7, 2023. A brief summary of the development of the NOAA-21 VIIRS version of the τ_{SDSM} is included in the following section with the improvements of the H-factor trends.

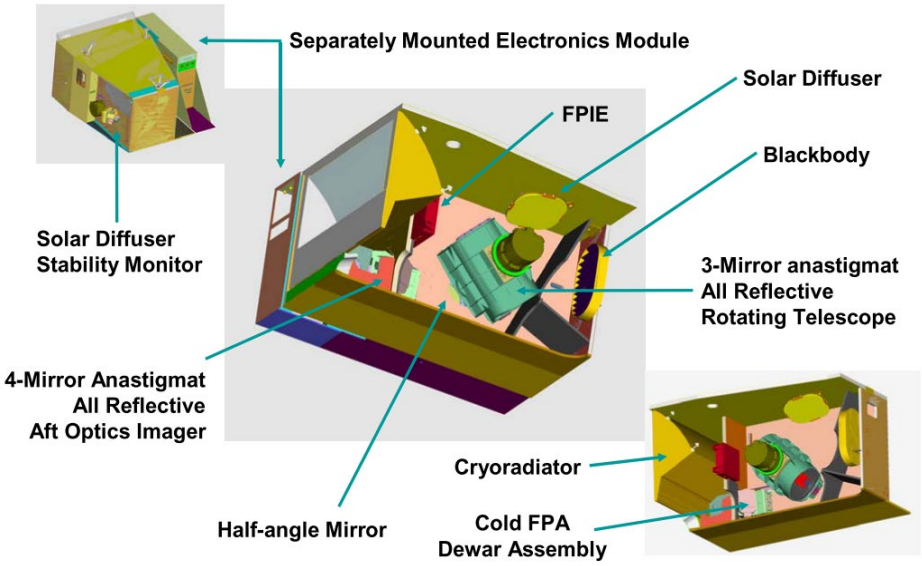

Figure 1. Simplified cut—out view of the VIIRS Opto-Mechanical Module (OMM) [9].

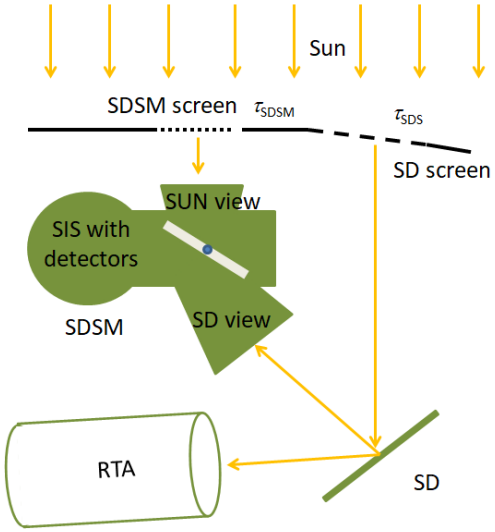

Figure 2. Operational schematics of VIIRS SDSM, SD, RTA, and screens relations[2].

To independently validate the VIIRS reflective solar bands (RSB), scheduled lunar observations are performed monthly and compared to the primary on-orbit SD calibrations. The spacecraft needs to perform a roll maneuver to place the moon at the center of the solar viewing (SV) port. On top of the roll maneuver, the sector rotation command is then used to shift the Earth viewing (EV) sector to the SV port location, so that users can have extended EV data through the SV port. Lunar irradiances are calculated from the lunar observations by applying the calibration coefficients and taking ratio them to the reference irradiance values from the Global Space-based Inter-Calibration System (GSICS) Implementation of ROLO (GIRO) model [10, 11]. It is a bit early stage of to compare the lunar calibration result by having only four collections but the primary lunar calibration results are discussed in this study.

For the NOAA-20 VIIRS case, there were growing discrepancies between the primary on-orbit SD calibrations and lunar calibrations, especially in the NOAA-20 VIIRS short wavelength bands (M1-M4). For NOAA-20 operational VIIRS RSB Sensor Data Record (SDR) products, small but meaningful upward trends were observed and applied in the

selective RSB bands. Similar to the previous applications, the on-orbit lunar calibration results are compared and discussed in this study for the best quality of the NOAA-21 VIIRS RSB calibration to the end users.

2. ON-ORBIT CALIBRATION METHODOLOGIES

2.1 On-orbit Solar Diffuser (SD) Calibration

Figures 1 and 2 illustrate the various view sources of the NOAA-20 VIIRS, which include Earth View (EV), backbody (BB), SD, and SDSM views. These on-board calibrators are observed by the Rotating Telescope Assembly (RTA) and Half Angle Mirror (HAM). The SD, SDSM, and SV views are utilized for RSB calibration, while the BB and SV views are employed for TEB calibration. During each anticlockwise rotation of the RTA, the VIIRS sequentially captures EV, BB, and SD views (along with the SDSM view, which requires a specific operational command). One of the main challenges in SD calibration is the gradual degradation of the SD surface's reflectance (referred to as Spectralon) due to exposure to strong ultraviolet light and high-energy particles[5]. These time-dependent changes in SD reflectance are monitored by the SDSM using eight different SDSM detectors located inside the SDSM Spherical Integrating Surface (SIS), as depicted in Figure 2.

Equation 1 demonstrates the calculation of the H-factor, which involves taking ratios between the bias removed digital count of SD (dc_{SD}) and the bias removed Sun digital count (dc_{SUN}). These ratios are adjusted using the corresponding corrections for the SDSM Sun screen transmittance function (τ_{SDSM}), the combined product of the SD BRDF function and the SD screen transmittance function ($\tau_{SD}BRDF_{SDSM}$), the cosine effect of the incoming sunlight incident on SD ($cos(\theta_{inc})$), and the solid angle of the SDSM view port (φ).

$$H(t) = \frac{dc_{SD}(t)\cdot\tau_{SDSM}(t)}{dc_{SUN}(t)\cdot BRDF_{SDSM}(t)\cdot\tau_{SDS}(t)\cdot cos(\theta_{inc})\cdot\pi\cdot sin^2\varphi} \quad (1)$$

Once the periodic SDSM measurements yield the H-factor, the primary on-orbit calibration coefficient, known as the F-factor, can be determined when the azimuth and elevation angles of Sun illumination on the SD screen fall within the desired range illustrated in Figure 2. This range, referred to as the 'sweet spot,' occurs approximately 14 or 15 times per day near the South Pole for a Sun-synchronous sensor [10]. The F-factors are calculated using Equation 2 below for each scan within the 'sweet spot' range.

$$F(t) = \frac{cos(\theta_{inc}(t))\cdot\left\{E_{sun}(t)\cdot\tau_{SDS}(t)\cdot BRDF_{RTA}(t)\cdot\frac{H(t)}{H(t_0)}\right\}\cdot RVS_{SD}}{C_0+C_1dn_{SD}(t)+C_2dn_{SD}^2(t)+C_3dn_{SD}^3(t)} \quad (2)$$

In the numerator of Equation 2, the cosine effect of the incident solar angle is adjusted by $cos(\theta_{inc}(t))$. E_{sun} represents the solar irradiance model spectrum convolved with the spectral response function, corrected for variations in the Sun-Earth distance. $\tau_{SDS}BRDF_{RTA}$ represents a combined function of the SD screen transmittance (τ_{SDS}) and the bidirectional reflectance distribution function (*BRDF*) of the SD surface at the RTA viewing angle. The normalized function of H(t) / H(t_0) provides the relative degradation of the SD in a specific RSB band at the center wavelengths. RVS_{SD} corresponds to the response versus scan angle (RVS) response at the SD angle on the HAM. The numerator of the F-factor equation establishes the reference radiance during SD observation by the VIIRS instrument. In the denominator of Equation 2, a cubic function of dn_{SD}(t) is employed, utilizing prelaunch c-coefficients. Lower-case letters indicate the removal of bias or offset from the detector response, with dn_{SD}(t) representing the digital number (DN). This cubic function, in conjunction with the SD response using the c-coefficients, determines the corresponding observed SD radiance by the VIIRS. The ratio between the theoretical reference radiance and the observed SD radiance by VIIRS detector constitutes the F-factor, as depicted in Equation 2. It is important to note that F-factors are computed separately for each band, detector, gain state, and HAM side.

2.2 On-orbit Lunar Calibration

The VIIRS instrument on the NOAA-21 satellite can view the Moon through its space view (SV) port before the start of its EarthView (EV) scan. About one month before a scheduled lunar observation, the NOAA VIIRS team uses software developed from the SPICE package of NASA's Jet Propulsion Laboratory's (JPL) Navigation and Ancillary Information Facility (NAIF) to predict possible lunar data collection opportunities.

The best scheduled lunar collection time is determined by validating the NOAA team's prediction results with those of the NASA VIIRS Calibration Support Team (VCST). Once there is a mutual agreement between the NASA and NOAA teams, the collection time and spacecraft roll angles are delivered to the NOAA Satellite Operational Facility (NSOF) to perform the scheduled lunar collection.

After the collection, the NOAA VIIRS team confirms the successful scheduled lunar collection by visually inspecting the lunar observations. Figure 3 shows an example of scheduled lunar collection images in all the RSB bands. For NOAA-20 and NOAA-21 VIIRS instruments, the Moon is located in the non-aggregation zone near the left edge of the EV scan by applying the sector rotation. However, the S-NPP places the Moon at the center of the EV frame, which is in the 3-sample aggregation zone[11].

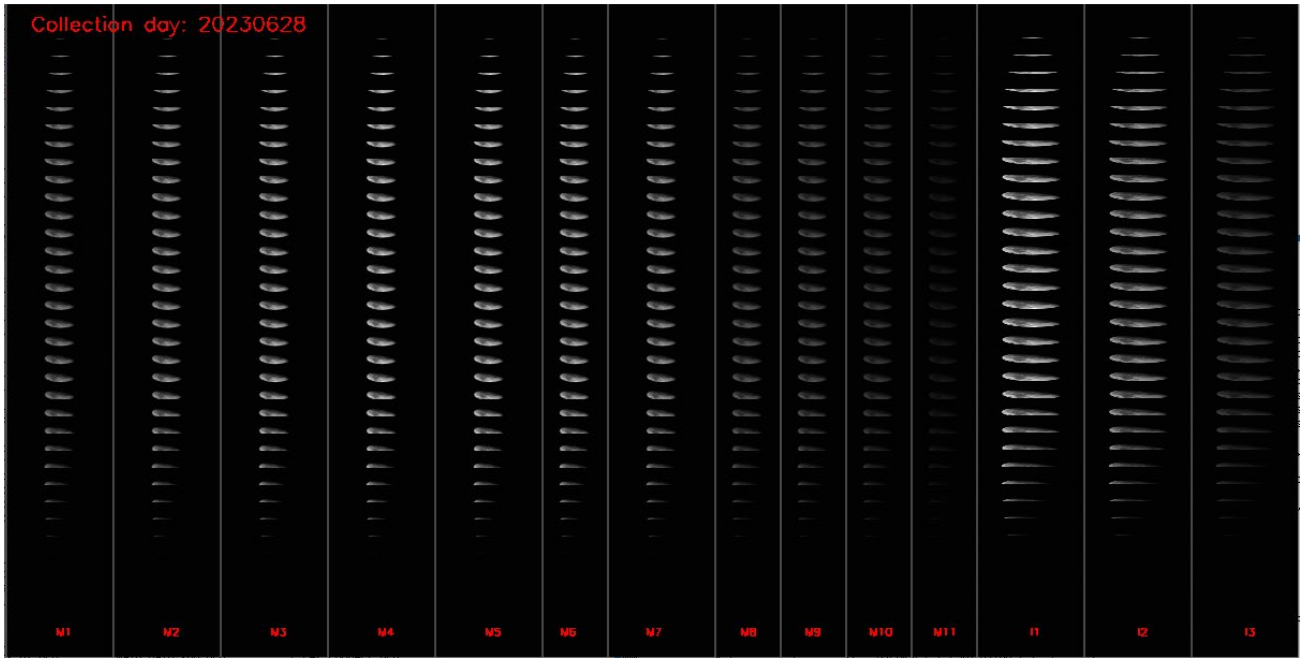

Figure 3. NOAA-21 VIIRS scheduled lunar collection on June 28, 2023 in the RSBs.

In addition to the VIIRS lunar observation, the expected lunar irradiance can be derived from the U.S. Geological Survey (USGS) Robotic Lunar Observatory (ROLO) model at the time of lunar collection. The GSICS (Global Space-based Interferometry for Climate Studies) team has implemented the ROLO model and released their implementation to the international agencies as the GIRO model. Theoretically, GIRO and ROLO should provide the same value but there were very small (less than 0.1% level), and GIRO is used for this work. The GIRO lunar irradiance model has been used for S-NPP [10, 12, 13]and NOAA-20 VIRIS [14]long-term on-orbit calibration comparisons between the solar diffuser (SD) and the Moon.

The GIRO irradiance is calculated for each lunar collection at the specific time of lunar observation, accounting for the removal of bias from the VIIRS detector response across bands, detectors, HAM sides, and scans (Equation 3). To determine the detector offsets, 100 frames away from the moon are averaged on both sides of the moon during each scan. It is important not to use the SV (Space View) responses to estimate the detector offset, as they are not valid during sector

rotation. Equation 3 represents the calculation of 'dn' (the bias removed value) by subtracting the average space DN from the lunar DN. Once 'dn' is obtained, Equation 4 is used to derive the radiance of the lunar pixels. This involves using prelaunch c-coefficients, RVS (Relative Viewing System) values, and fixed SD (Solar Diffuser) F-factors.

$$\mathrm{dn} = DN_{moon} - \overline{DN_{Space}} \tag{3}$$

$$L_{pixel} = F_{SD} \cdot \{c_0 + c_1 dn + c_2 dn^2 + c_3 dn^3\} / RVS_{SV} \tag{4}$$

Starting from NOAA-20 (or JPSS-1) VIIRS, a cubic function is employed for radiance calculation, particularly for the SWIR (Short-Wave Infrared) bands. It's worth noting that Equations 3 and 4 are simplified and do not explicitly mention the time-dependent details for each band, detector, HAM side, and scan. In the RSB (Reflective Solar Bands) band calibration, all c0 values are set to zero, whereas non-zero c0 values are used for the thermal band radiance calibration.

After calculating the non-zero radiance values for the lunar pixels, Equation 5 is used to determine the observed lunar irradiance and the lunar F-factor of the collection. Equation 5's bottom part represents the observed lunar irradiance, which is derived from the lunar radius (Rmoon), the distance between the satellite and the moon (DSat_Moon), the lunar phase angle (θ), the accumulated observed lunar radiance (Lpixel), and is divided by the effective number of lunar pixels (N).

$$F_{lunar} = \frac{I_{GIRO}}{I_{OBS}} = \frac{I_{GIRO}}{\frac{\pi \cdot R_{moon}^2}{D_{Sat\_Moon}^2} \cdot \frac{1+\cos(\theta)}{2} \cdot \sum_{Pixel} \frac{L_{Pixel}}{N}} \tag{5}$$

3. RESULTS

3.1 On-orbit Solar Diffuser (SD) Calibration Results

3.1.1 Initial H-factor and F-factors

The initial NOAA-21 VIIRS H-factors were calculated by using the prelaunch SDSM LUTs. As shown in Figure 2 and Equation 1, the SDSM Sun screen transmittance function (τ_{SDSM}) and the combined product of the SD BRDF function and the SD screen transmittance function ($\tau_{SD}BRDF_{SDSM}$) are used. Figure 4 shows the initial NOAA-21 VIIRS H-factors in all the SDSM detectors. In all SDSM detectors, there were more than 1 percent levels of oscillations. These initial oscillations were also observed in S-NPP and NOAA-20 VIIRS instruments [8, 15]. The main source of the oscillations is caused by incorrect prelaunch measurement of τ_{SDSM} LUT.

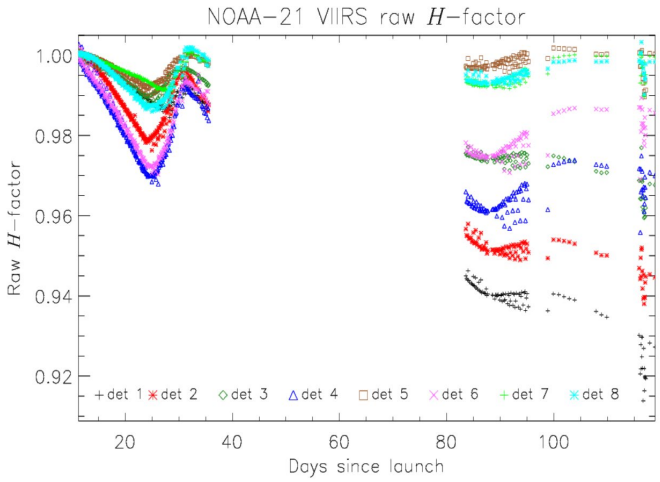

Figure 4. NOAA-21 VIIRS initial H-factors using prelaunch SDSM LUTs. The data gap between DSL 35 to 82 indicates satellite Ka band transmittance (TX) antenna anomaly period.

To estimate a new τ_{SDSM} function, a series of NOAA-21 VIIRS 14 yaw maneuvers were performed on 3/6 and 37/2023. In Figure 4, the yaw maneuver points near Day Since Launch (DSL) 117 showed approximately 1.5% level in all the detectors which proves the problem of the τ_{SDSM} LUT. Due to the oscillation problem, the initial H-factor was set to unity for the SD F-factor calculation. Figure 5 shows NOAA-21 VIIRS initial on-orbit calibration coefficients called F-factors with H=1 all the time.

Especially in the shortwave VISNIR bands, the slopes of the H-factors were increased toward the short side of the wavelength. The corresponding normalized plot on the right M1 showed almost 5.5 percent changes near DSL 90, whereas almost no changes in band M7. These F-factor changes were caused by the non-unity H-factors and the changes in the shortwave bands were mostly caused by the H-factor changes.

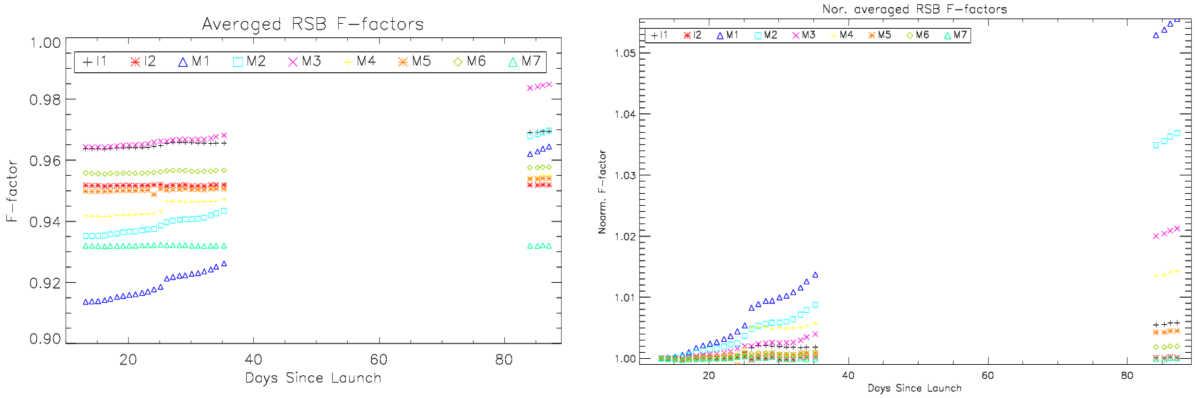

Figure 5. NOAA-21 VIIRS initial F-factors using H=1.

3.1.2 H-factor update from the yaw-maneuvers

The NOAA VIIRS SDR team calculated the desired 15 yaw angles over the 15 orbits as shown in Figure 6. The yaw angles need to be predicted approximately 20 days ahead of the satellite mission operation team's schedule. It requires prediction of the spacecraft yaw angles and timing of the maneuvers for the best solar azimuth angles on the SDSM sun screen. There were 14 yaw maneuvers with one normal SDSM collection from 3/6/2023 to 3/7/2023 from orbit number 1649 to 1663 with a regular SDSM collection without yaw in the orbit number of 1654. For each yaw maneuver, there was a 5-minute SDSM measurement that should start 2 minutes before the desired center time.

A new version of LUT was calculated only using yaw maneuver results and re-calculated the H-factors. The updated H-factors with the updated τ_{SDSM} LUT are shown in Figure 7. Compared to the initial H-factor using the prelaunch LUTS, the H-factor oscillations were significantly reduced especially in the early stage of H-factors from 0 to 40 DSL.

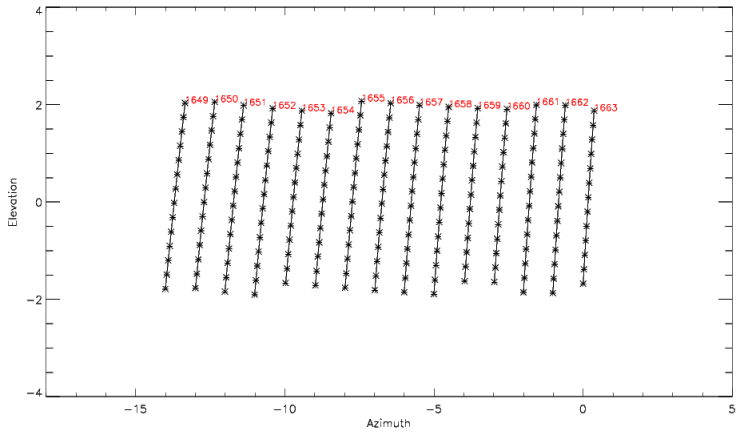

Figure 6. NOAA-21 VIIRS SDSM solar screen azimuth and elevation angles with the 15-yaw maneuvers over March 6-7, 2023 within the operational SDSM solar ranges.

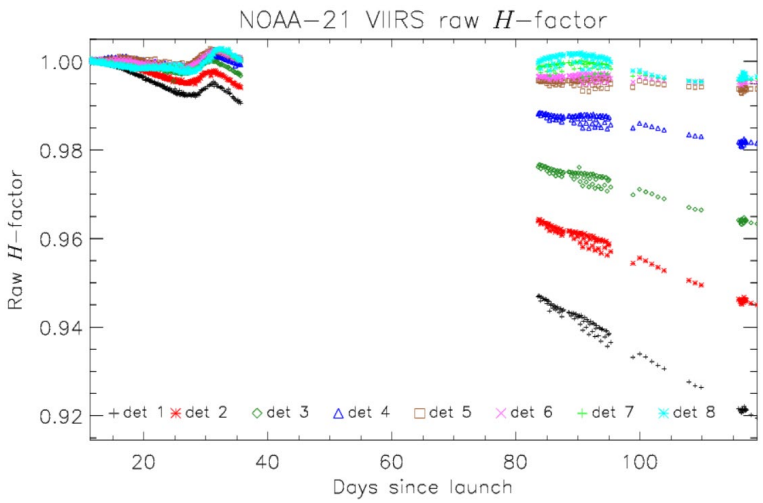

Figure 7. NOAA-21 VIIRS H-factor with yaw maneuver derived τ_{SDSM} LUT.

3.1.3 H-factor update from the yaw-maneuver and on-orbit SDSM data

After the first update of the τ_{SDSM} LUT, the on-orbit SDSM data sets were added in between the yaw-maneuver points. Figure 8 shows the on-orbit SDSM data sets in blue vertical lines and the yaw-maneuver data sets were indicated by red lines. The symbols in Figure 8 represent the sun view portion of the SDSM data. In each orbit, the solar elevation values were rapidly changed according to the sun position and Figure 8 only shows the operational solar elevation angles from -2 to 2 degrees. But the solar azimuth angles slowly changed along with the time of the year. The NOAA-21 VIIRS SDSM solar azimuth angles are shown in Figure 9 and by June 27, 2023, the on-orbit SDSM data filled up until -13 degrees starting from -1 degrees since November 20, 2022.

Another version of the τ_{SDSM} LUT was derived from the combined yaw maneuver and on-orbit SDSM data sets and applied to the H-factor calculation. Figure 10 shows the first version of the latest version of the H-factor with yaw and on-orbit SDSM data until /23/2023 (DSL 155) in (a) and 6/27/2023 (DSL 230) in (b).

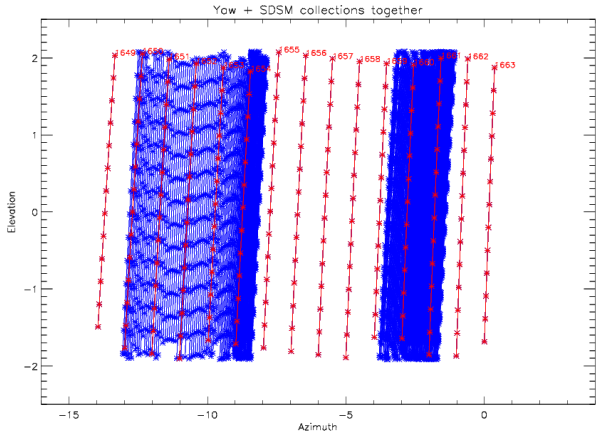

Figure 8. NOAA-21 VIIRS SDSM solar screen azimuth and elevation angles with the 15 yaw maneuvers (red lines) and on-orbit SDSM data (vertical blue lines) set from 11/20/2022 to 6/27/2023.

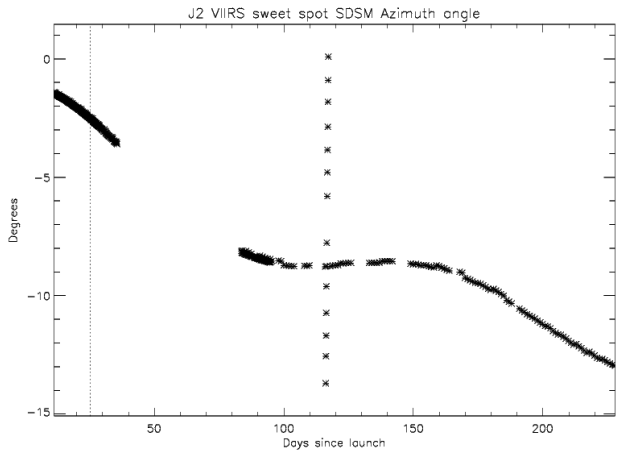

Figure 9. NOAA-21 VIIRS SDSM solar screen azimuth and elevation angles with the 15 yaw maneuvers (red lines) and on-orbit SDSM data (vertical blue lines) set from 11/20/2022 (DSL 10) to 6/27/2023 (DSL 230).

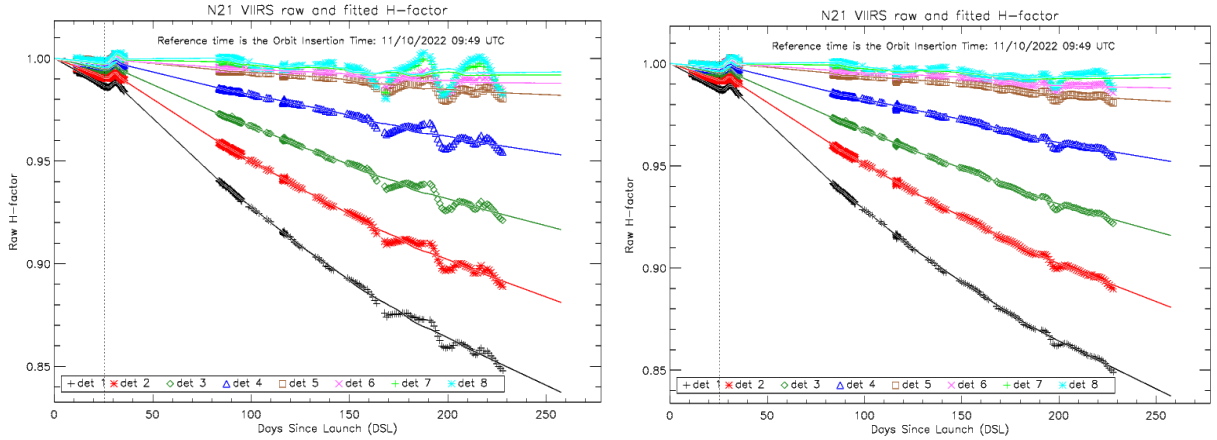

(a) On-orbit SDSM data until 4/23/2023 (b) On-orbit SDSM data until 6/27/2023

Figure 10. NOAA-21 VIIRS H-factor with the τ_{SDSM} LUT from yaw and on-orbit SDSM data until 4/23/2023 (DSL 155) and H-factor with the τ_{SDSM} LUT from yaw and on-orbit SDSM data until 6/27/2023 (DSL 230).

The τ_{SDSM} LUT using on-orbit data until 4/23/2023 did not provide stable H-factors beyond 160 since it did not provide fine features in between the yaw maneuver points. The newly updated τ_{SDSM} LUT using on-orbit data until 6/27/2023 showed a much more stable response than the previous version in Figure 10 (a). According to the annual pattern of the solar azimuth angle in Figure 9, the on-orbit SDSM data will be filled up by the end of 2023 and the H-factors will be newly updated around the time of the year.

3.1.4 On-orbit SD F-factors

Once the H-factors were successfully derived with the yaw and on-orbit SDSM data, the SD F-factors could be calculated from Equation 2. The F-factors are very stable over time in the VISNIR bands (M1~M7, I1, and I2), whereas SWIR band gains are rapidly changing over time. The SWIR band gain degradation (or increase of the F-factors) was captured and timely updated the operational F-factors.

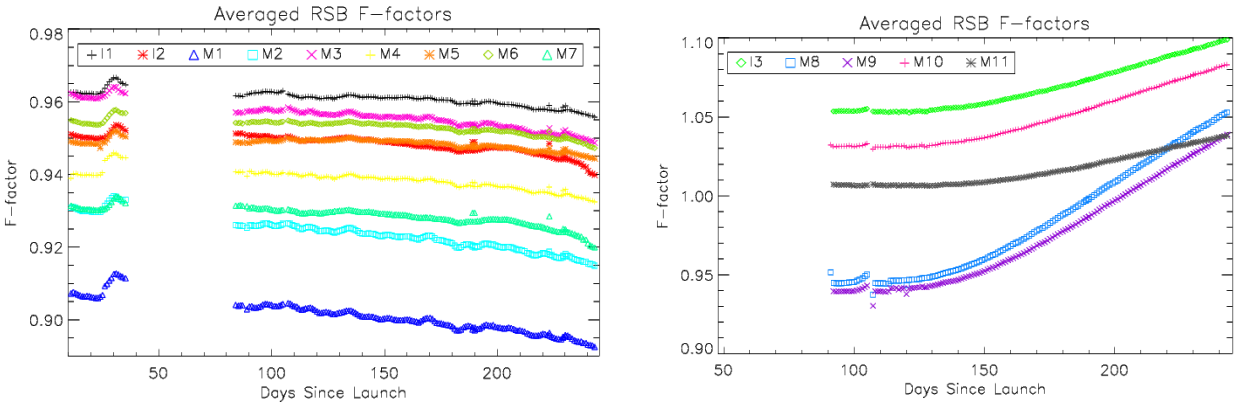

(a) VISNIR bands (M1~M7, I1, and I2)

(b) SWIR bands (M8~M11, and I3)

Figure 11. NOAA-21 VIIRS offline SD F-factors in VISNIR and SWIR bands.

3.1.5 Operational F-factor updates

The pre-launch calibration coefficients for the VNIR bands were applied in the VIIRS SDR production at NOAA IDPS until the update on Jan. 12, 2023. Those coefficients were derived from the measurements conducted by the VIIRS manufacturer to verify instrument performance before the launch of the satellite. The first update of the coefficients was derived from the on-orbit solar calibration measurements acquired for the VNIR bands. While all solar calibration data acquired since the VIIRS activation were reanalyzed, only the F factors from the following time span were used to derive the updated values: Dec. 11-14, 2022. The limited time span of the selected data was due to the prolonged spacecraft orbit phasing (raising) campaign and the sudden interruption of the solar calibration data availability after the NOAA-21 satellite Ka-band transmitter anomaly on Dec. 16, 2022. Because of the uncertainty in the SD reflectance monitoring, degradation of the SD reflectance was at first omitted in the analysis (by setting H = 1), and then approximately accounted for by extrapolating the trends to the launch date, under the assumption that the observed trends are not due to degradation of the VIIRS radiometric response, but rather they are only due to the SD degradation. The extrapolation created corrections that were the largest for bands M1 and M2, about 2%, as shown for band M2 in Figure 12. There were no further updates of the F factors for VNIR bands, based on the relative stability of the Earth observations in these bands so far.

While the SWIR band data became available in February 2023, the detector temperature stabilized only on March 4, 2023, following a mid-mission outgassing and the temperature setpoint changed from 82 K to 80 K. Calibration coefficients for the SWIR bands were updated for the first time after launch on Mar. 23, 2023. Shortly thereafter, SWIR-band radiometric response degradation was detected, and the F factors were subsequently updated on Apr. 20, May 11, June 1, and June 23, 2023, with plans to update them with an approximately monthly frequency until an automated solar calibration procedure is applied in the IDPS production of VIIRS SDR for the SWIR bands. A quadratic extrapolation is used to predict the F factor values between the periodic updates. Figure 13 shows the F factor changes for the SWIR band the most affected by the degradation: M8. The degradation is not only band-dependent, but even more strongly detector-dependent. If not corrected with the F factor updates, the degradation would create noticeable striping in the SWIR-band images. As of this writing, the root cause of the degradation is still under investigation. Figure 13 also shows an example of the predicted F factors that were applied in the VIIRS SDR processing between May 11 and June 1, 2023.

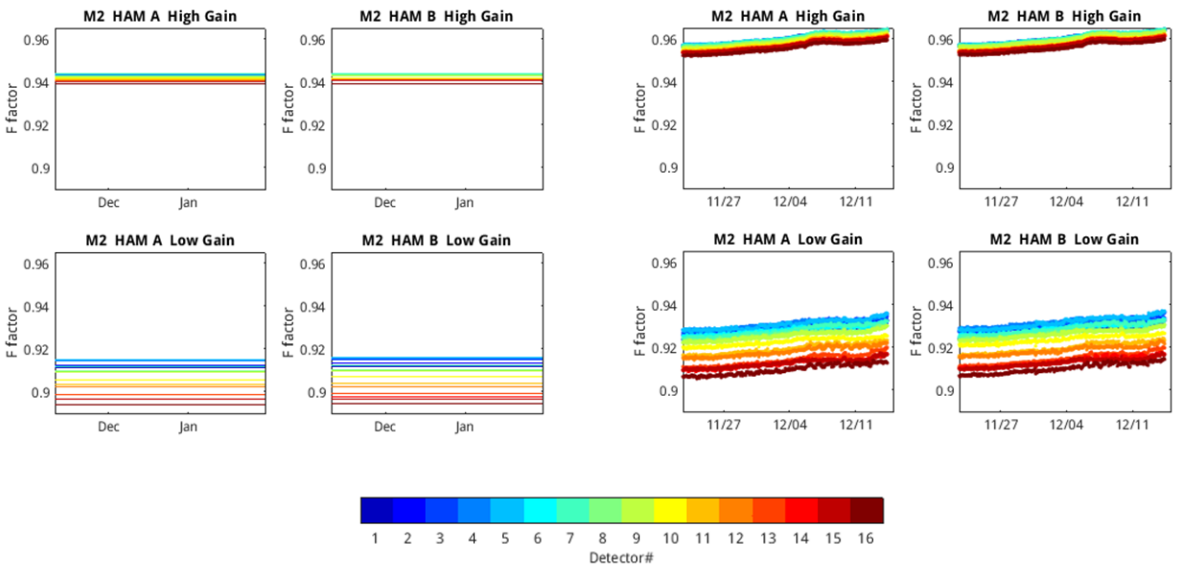

Figure 12. NOAA-21 VIIRS band M2 F factors calculated from the solar calibration data with the SD degradation omitted (right panel) and extrapolated to the satellite launch date (left panel), generating the constant values applied in the SDR processing.

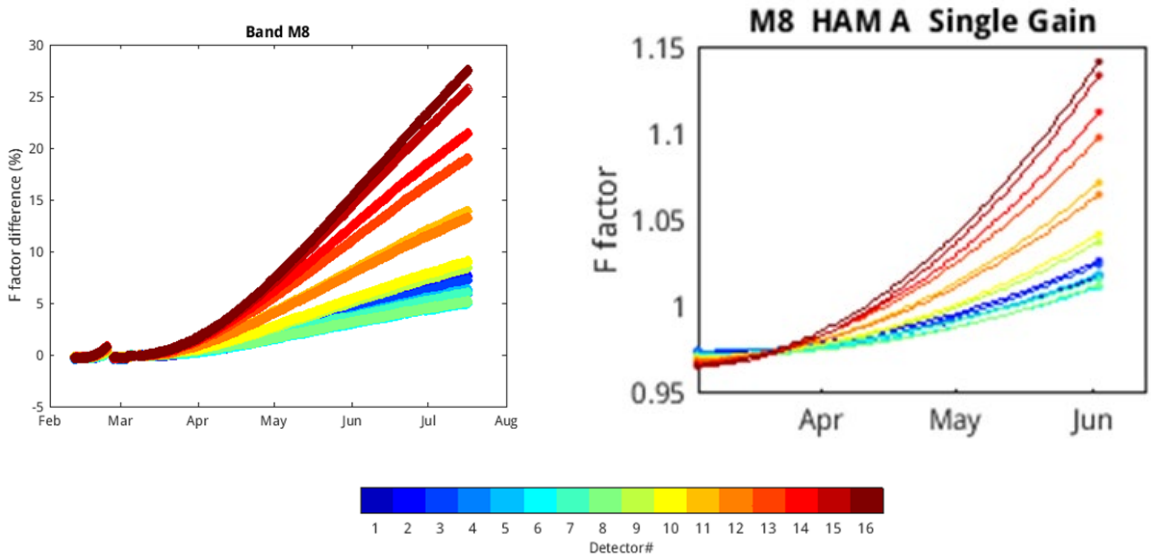

Figure 13. NOAA-21 VIIRS band M8 F-factor changes were calculated from the solar calibration data (left graph) and the respective F factor values applied in the IDPS processing between May 11 and June 1, 2023 (right graph).

While initial Earth observations showed a satisfactory agreement between the VIIRS SWIR-band measurements from NOAA-20 and NOAA-21 when the pre-launch calibration was applied for the latter, significant biases became apparent after the first post-launch F factor update. To improve agreement between Earth observations in the SWIR bands from NOAA-21 and NOAA-20, the following bias corrections have been applied in the NOAA-21 VIIRS SDR production at IDPS since May 11, 2023 (June 23, 2023 for M9):

- +1.5% for band I3
- +2.0% for bands M8 and M9
- +2.5% for M10
- +4.0% for M11

3.2 On-orbit lunar calibration Results

There were 5 scheduled lunar collections as shown in Table 2 with dates of scheduled lunar collection, center collection time in UTC, and lunar phase angles of the moon. Similar to the NOAA-20 VIIRS case, the location of the observed moon of the NOAA-21 VIIRS scheduled lunar collection is in the non-aggregation zone. The desired lunar phase angle is -51 degrees but the first and last one is -8 degrees away from the desired phase angle that can cause different uncertainty from the lunar phase angle. For the five collections, three collections (4/1, 5/31, and 6/28) were spacecraft roll-maneuver free collections which may not guarantee the location of the moon in the EV frame. Due to the possible random position of the moon, the uncertainty of the moon calibration could be increased. For the 4th scheduled lunar collection on 5/31/2023, the moon appeared in the center of the SV port even though it was a roll-maneuver free collection.

Table 2. Scheduled lunar collection for NOAA-21 VIIRS.

Date	Time [UTC]	Lunar phase angle
3/2/2023	01:23:47	-59.43
4/1/2023*	10:42:07	-52.97
5/1/2023	08:05:33	-51.13
5/31/2023*#	00:27:01	-50.99
6/28/2023*	20:29:43	-59.99

*No lunar roll maneuver was performed. # Moon appeared in nominal location.

As shown in Figure 14, the lunar F-factors were very consistent within one percent level especially in the VISNIR bands (M1~M7, I1 and I2) compared to the on-orbit SD F-factors. The lunar F-factors were normalized to the SD F-factors on the first date of 3/2/2023 because there were large initial offsets between the SD and lunar F-factors due to the solar irradiance model differences [11]. There were growing differences between the SD and lunar F-factors especially in the short wavelength band in M1 (black colored symbols and lines) and M2 in red color in Figure 14. These short wavelength deviations were also observed and effectively corrected with the NOAA-20 VIIRS case. These differences were caused by the estimated H-factor (SD degradation) differences between the center wavelength based algorithm and considering the whole spectral response function [16]. A new version of the H-factor difference simulation between center wavelength and spectral response function with the surface roughness Rayleigh scattering (SRRS) model [5] will be performed soon to mitigate these differences.

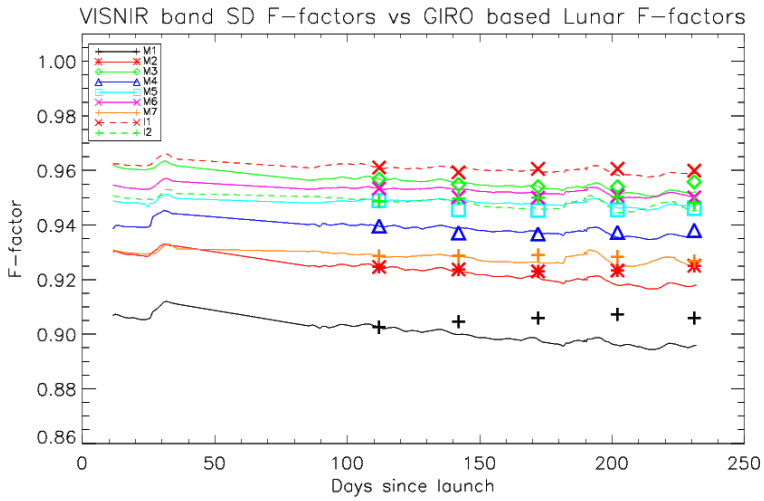

Figure 14. NOAA-21 VIIRS initial SD and lunar F-factor trend comparisons in VISNIR bands.

When it comes to the NOAA-21 VIIRS SWIR bands, significant time-dependent detector degradations were observed as mentioned in the SD F-factor results (in section 3.14). The SWIR band lunar F-factors also showed very similar increases of the F-factors but not as fast as the SD F-factors showed as shown in Figure 15. Large degradations of more than seven percent were observed in bands M8 and M9. In all the SWIR bands, lunar F-factors showed slightly less than the SD F-factors as shown in Figure 15 (b).

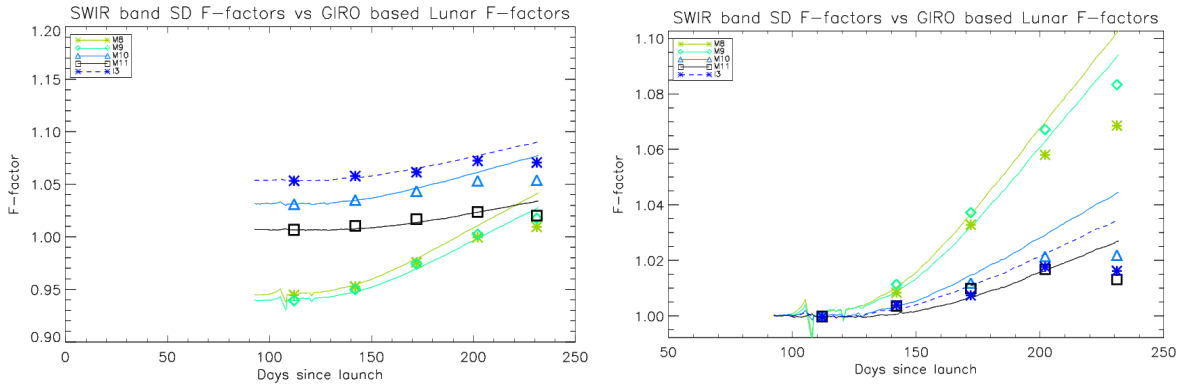

(a) Lunar F-factors are normalized to the SD F-factors (b) Normalized to the first point of SD F-factors

Figure 15. NOAA-21 VIIRS initial SD and lunar F-factor trend comparisons in SWIR bands.

4. SUMMARY

The NOAA-21 VIIRS was successfully launched on November 10, 2022 and went through extensive post-launch tests. It was found that the VIIRS instrument is performing well in the RSB. Similar to the NOAA-20 VIIRS case, the initial H-factor showed significant levels of oscillations up to 1.5 percent due to the improper measurements of the prelaunch SDSM sun transmittance LUT. Because of the H-factor instability, it was assumed that there was no SD degradation by setting the H-factor equal to one initially, and estimated the corresponding initial SD F-factors for the VIIRS SDR production. As expected, the H-factor oscillations were mitigated by a series of yaw maneuvers which were performed over March 6 to 7, 2023 but not completely resolved oscillation issues. The on-orbit SDSM data sets were used to fill up the SDSM solar azimuth gaps since launch but it will be completed by the end of this year to cover the full range of the solar azimuth angles. With an intermediate version of the SDSM sun transmittance function, the offline F-factors were calculated and compared to the lunar F-factors. As we expected the lunar F-factors showed very consistent half-year trends along with the offline SD F-factors. The lunar F-factors tracked the changes in the SWIR band gain degradation (or increases of the F-factors) effectively.

For operational product, constant F-factors were used in VISNIR bands which are validated by the stable lunar F-factors. On the other hand, the SWIR band time and detector dependent degradations were observed and mitigated by a series of calibration coefficient updates from March 23, April 29, May 11, June 1 and June 23, 2023. In addition to these calibration coefficient updates, the NOAA VIIRS SDR team is currently testing automated solar calibration for the future VIIRS SDR production which will require further investigations of the on-orbit calibration changes and mitigation algorithms. Currently, the SWIR band calibration coefficients are within 0.2 percent accuracy level compared to the SD calibration. The NOAA VIIRS SDR calibration team will continue to validate the long-term trends in comparison with the long-term lunar, Deep Convective Cloud, and Simultaneous Nadir Observations trending results for the best quality of the products.

5. ACKNOWLEDGEMENTS

Authors appreciate detailed technical guidance and excellent leadership from Dr. Changyong Cao as the NOAA VIIRS SDR team lead and Sensors and Calibration Branch Chief at NOAA STAR.

6. DISCLAIMER

The scientific results and conclusions, as well as any views or opinions expressed herein, are those of the author(s) and do not necessarily reflect those of NOAA or the Department of Commerce.

REFERENCES

[1] C. Cao, F. J. De Luccia, X. Xiong, R. Wolfe, and F. Weng, "Early On-Orbit Performance of the Visible Infrared Imaging Radiometer Suite Onboard the Suomi National Polar-Orbiting Partnership (S-NPP) Satellite," *IEEE Transactions on Geoscience and Remote Sensing,* vol. 52, no. 2, pp. 1142-1156, 2014.

[2] C. Cao *et al.*, "NOAA-20 VIIRS on-orbit performance, data quality, and operational Cal/Val support," in *SPIE Asia-Pacific Remote Sensing*, 2018, vol. 10781, p. 9: SPIE.

[3] G. Thuillier *et al.*, "The Solar Spectral Irradiance from 200 to 2400 nm as Measured by the SOLSPEC Spectrometer from the Atlas and Eureca Missions," *Solar Physics,* vol. 214, no. 1, pp. 1-22, 2003/05/01 2003.

[4] D. Moyer *et al.*, "JPSS-1 VIIRS Prelaunch Reflective Solar Band Testing and Performance," *Remote Sensing,* vol. 14, no. 20, 2022.

[5] X. Shao, T.-C. Liu, X. Xiong, C. Cao, T. Choi, and A. Angal, "Surface Roughness-Induced Spectral Degradation of Multi-Spaceborne Solar Diffusers Due to Space Radiation Exposure," *IEEE Transactions on Geoscience and Remote Sensing,* pp. 1-14, 2019.

[6] X. Shao, C. Cao, and T.-C. Liu, "Spectral Dependent Degradation of the Solar Diffuser on Suomi-NPP VIIRS Due to Surface Roughness-Induced Rayleigh Scattering," *Remote Sensing,* vol. 8, no. 3, 2016.

[7] T. Choi, C. Cao, S. Blonski, W. Wang, S. Uprety, and X. Shao, "NOAA-20 VIIRS Reflective Solar Band Postlaunch Calibration Updates Two Years In-Orbit," *IEEE Transactions on Geoscience and Remote Sensing,* pp. 1-10, 2020.

[8] T. Choi, X. Shao, S. Blonski, and C. Cao, "On-orbit NOAA-20 VIIRS solar diffuser bidirectional reflectance distribution function and screen transmittance characterization using yaw manoeuvres and regular on-orbit SDSM data," *International Journal of Remote Sensing,* vol. 41, no. 17, pp. 6503-6526, 2020/09/01 2020.

[9] N. Baker and H. Kilcoyne, "Joint Polar Satellite System (JPSS) VIIRS Radiometric Calibration Algorithm Theoretical Basis Document (ATBD)," J. P. S. S. J. G. Project, Ed., ed. NOAA and NASA: NOAA & NASA, 2011.

[10] T. Choi, C. Cao, X. Shao, and W. Wang, "S-NPP VIIRS Lunar Calibrations over 10 Years in Reflective Solar Bands (RSB)," *Remote Sensing,* vol. 14, no. 14, 2022.

[11] T. Choi, X. Shao, S. Blonski, W. Wang, S. Uprety, and C. Cao, "NOAA-20 VIIRS initial on-orbit radiometric calibration using scheduled lunar observations," presented at the Earth Observing Systems XXIV, 2019.

[12] T. Choi, X. Shao, and C. Cao, "On-orbit radiometric calibration of Suomi NPP VIIRS reflective solar bands using the Moon and solar diffuser," *Appl Opt,* vol. 57, no. 32, pp. 9533-9542, Nov 10 2018.

[13] T. Choi, X. Shao, C. Cao, and F. Weng, "Radiometric Stability Monitoring of the Suomi NPP Visible Infrared Imaging Radiometer Suite (VIIRS) Reflective Solar Bands Using the Moon," *Remote Sensing,* vol. 8, no. 1, 2015.

[14] T. Choi and C. Cao, "NOAA-20 VIIRS On-Orbit Geometric Data Quality Estimation Using the Scheduled Lunar Collections," *IEEE Transactions on Geoscience and Remote Sensing,* vol. 60, pp. 1-10, 2022.

[15] T. Choi and C. Cao, "S-NPP VIIRS On-Orbit Calibration Coefficient Improvements With Yaw Maneuver Reanalysis," *IEEE Transactions on Geoscience and Remote Sensing,* vol. 57, no. 10, pp. 7460-7465, 2019.

[16] T. Choi and C. Cao, "NOAA-20 VIIRS Relative Spectral Response Effects on Solar Diffuser Degradation and On-Orbit Radiometric Calibration," *IEEE Transactions on Geoscience and Remote Sensing,* pp. 1-7, 2021.